Nonsequential triple ionization in strong fields

Krzysztof Sacha[1,2] and Bruno Eckhardt[1]
[1]*Fachbereich Physik, Philipps Universität Marburg, D-35032 Marburg, Germany*
[2]*Instytut Fizyki im. Mariana Smoluchowskiego, Uniwersytet Jagielloński, ulica Reymonta 4, PL-30-059 Kraków, Poland*
(Received 19 May 2001; published 2 October 2001)

We consider the final stage of triple ionization of atoms in a strong linearly polarized laser field. We propose that for intensities below the saturation value for triple ionization the process is dominated by the simultaneous escape of three electrons from a highly excited intermediate complex. We identify within a classical model two pathways to triple ionization, one with a triangular configuration of electrons and one with a more linear one. Both are saddles in phase space. A stability analysis indicates that the triangular configuration has the larger cross sections and should be the dominant one. Trajectory simulations within the dominant symmetry subspace reproduce the experimentally observed distribution of ion momenta parallel to the polarization axis.

DOI: 10.1103/PhysRevA.64.053401 PACS number(s): 32.80.Rm, 32.80.Fb, 05.45.Mt

I. INTRODUCTION

Multiple ionization is a fundamental process in laser-atom interactions [1,2]. It received particular attention when it was realized [3] that the cross section was much larger than could be expected from the independent electron model [1,2]. One therefore came to distinguish two modes of multi-ionization, a sequential ionization process that is compatible with an independent electron model, and a nonsequential one, where correlations in electron dynamics are important. The way interactions come in is a matter of debate but the rescattering model [4,5] has a fascinating combination of quantum tunneling and classical dynamics of electrons in a field and has the strongest support from experimental observations, theoretical analyses, and numerical simulations [1–20]. One consequence of the rescattering model is that the final decay toward multiple ionization is preceded by the formation of a highly excited complex of electrons close to the nucleus. This compound state forms during the collision of the rescattered electron with the core. In our analysis we take this state as the initial condition for the final decay toward a multiply ionized atom.

The way two electrons escape from this compound state in nonsequential double ionization has been elucidated in a recent set of experiments by Weber *et al.* [9]. They found that the electrons escape preferentially with the same momenta. This observation prompted us to analyze the classical pathways that could lead to double ionization [21,22]. In an extension of Wannier's analysis [23–27] we found that for two-electron escape most classical paths lie near a subspace of electrons moving at the same distance from the nucleus but reflection symmetric with respect to the field axis. Calculations of ion momenta parallel and perpendicular to the field within this subspace [21,22] are in favorable agreement with experiment.

At these laser intensities more than two electrons can also escape simultaneously. In particular, triple ionization has been investigated by Moshammer *et al.* [11] and the recoil ion momentum distributions have been measured. It is our aim here to present the extension of the previous arguments [21,22] to the case of triple ionization. We identify saddles for nonsequential three-electron escape and the relevant symmetry subspaces in which the saddles are situated. Numerical simulations within the subspaces allow us to obtain the ion momenta that result from simultaneous triple ionization. Specifically, in Sec. II we discuss the pathways that lead to triple ionization, identify two saddle configurations, and analyze their stability properties. In Sec. III we then present numerical results for the distributions of ion momenta within these two subspaces and compare them to the experimentally observed distributions. Finally, in Sec. IV we draw conclusions and given an outlook for higher multiple ionization.

II. PATHWAYS TO NONSEQUENTIAL TRIPLE IONIZATION

As in the case of double ionization we can assume that the electron dynamics during the final decay is fast compared to the changes in the field [21,22]. Then the straightforward extension of the double ionization analysis [21,22] to three-electron escape calls for an investigation of the stationary configurations of three electrons in an atom exposed to a strong static field. Keeping a high symmetry between the electrons, an obvious candidate is a configuration where electrons are placed at the vertices of an equilateral triangle whose plane is perpendicular to the field axis (see Fig. 1). Deviations from this plane, in particular, displacements in the field direction, will again be amplified by electron repulsion, thus leading to electrons being pushed toward the nucleus and not to triple ionization. This configuration has C_{3v} symmetry and will be analyzed in Sec. II A.

Further investigations show, however, that there is a second stationary configuration. This second configuration has all the electrons in a plane with one electron on the field axis and the others symmetric with respect to it. This configuration is of symmetry C_{2v} and will be analyzed in Sec. II B. The decay signatures of the two configurations are different and the experimental observations can be used to decide between them.

In both cases we start from the Hamiltonian for three electrons in a neutral atom in a laser field polarized along the z axis. Within the dipole approximation, with an infinitely heavy nucleus and in atomic units, the Hamiltonian is

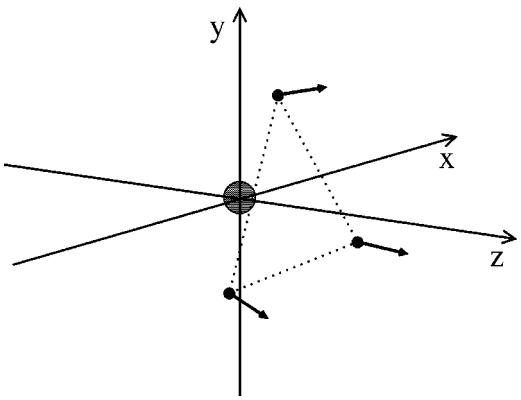

FIG. 1. Schematic representation of electron motion in the C_{3v} symmetry subspace. The electrons are placed in a plane perpendicular to the field polarization axis at the vertices of an equilateral triangle with the field axis in the center. The circle at the origin of the coordinate system marks the position of the nucleus.

$$H=\frac{1}{2}(\mathbf{p}_1^2+\mathbf{p}_2^2+\mathbf{p}_3^2)+V(\mathbf{r}_1,\mathbf{r}_2,\mathbf{r}_3,t), \tag{1}$$

with the potential energy

$$V=-\frac{3}{r_1}-\frac{3}{r_2}-\frac{3}{r_3}+\frac{1}{|\mathbf{r}_1-\mathbf{r}_2|}+\frac{1}{|\mathbf{r}_2-\mathbf{r}_3|}+\frac{1}{|\mathbf{r}_1-\mathbf{r}_3|} -(z_1+z_2+z_3)Ff(t) \tag{2}$$

and the time dependence of the pulse

$$f(t)=\sin^2(\pi t/T_d)\cos(\omega t+\phi). \tag{3}$$

F, T_d, ω, and ϕ stand for peak amplitude, duration, frequency, and phase of the external field, respectively.

The projection of total angular momentum onto the polarization axis is conserved so that the number of degrees of freedom is reduced by one, leaving eight plus the time dependence from the external field. We work in a subspace where this component vanishes.

Before we proceed with our analysis, note a scaling symmetry of the classical Hamiltonian (1) that can be used to eliminate one parameter. If the variables are rescaled according to

$$\begin{aligned} H&=F^{1/2}H', \\ \mathbf{r}&=F^{-1/2}\mathbf{r}', \\ \mathbf{p}&=F^{1/4}\mathbf{p}', \\ t&=F^{-3/4}t', \\ \omega&=F^{3/4}\omega', \end{aligned} \tag{4}$$

the dynamics becomes independent of the peak field amplitude, i.e., the system is described by the Hamiltonian (1) with $F=1$. We will use this scaling, but drop the prime to denote the scaled variables, for the analysis of the saddles, but we will keep the full field dependence for the dynamical simulations.

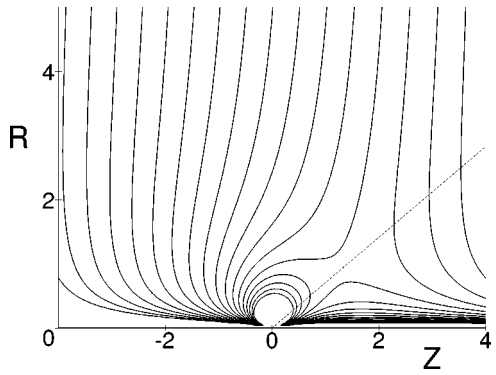

FIG. 2. Equipotential curves of the potential energy (6) for three electrons. The potential is plotted for a field strength $Ff(t)=1$. The saddles move along the dashed line when the electric field points in the positive z direction and along the one obtained by reflections in $z=0$ during the other half of the field cycle.

A. C_{3v} symmetry subspace

For zero total angular momentum projection on the polarization axis, the C_{3v} symmetric configuration corresponds in cylindrical coordinates to electron positions given by $z_i=Z$, $\rho_i=R$, and $\varphi_i=2\pi i/3$ with conjugate momenta $p_{z_i}=p_Z/3$, $p_{\rho_i}=p_R/3$, and $p_{\varphi_i}=0$, respectively. The Hamiltonian of the system in the C_{3v} subspace then reads

$$H(p_R,p_Z,R,Z,t)=\frac{p_R^2+p_Z^2}{6}+V(R,Z,t), \tag{5}$$

with potential energy

$$V=-\frac{9}{\sqrt{R^2+Z^2}}+\frac{3}{2R\sin(\pi/3)}-3Zf(t). \tag{6}$$

The three terms in Eq. (6) are the cumulative interaction of three electrons with the triply charged nucleus, the repulsion energy between electrons at distances $2R\sin(\pi/3)$, and the interaction with the external field, respectively. The variables are scaled according to Eq. (4) so that the field amplitude F is absent.

Electron motion close to the nucleus is much faster than the change of the phase of the laser field applied in the experiments [7–11,21,22]. Therefore, we can use an adiabatic approximation and gain insight into the qualitative features of the ionization process by analyzing the potential (6) for fixed external field. Note, however, that we use the full time dependence for the determination of the final ion momenta below. The potential (6) for a given time and thus a fixed value of $f(t)$ is shown in Fig. 2. The saddle is located along the lines $Z_s=r_s\cos\theta_s$ and $R_s=r_s\sin\theta_s$ with $\theta_s=\theta$ or $\theta_s=\pi-\theta$, where

$$\theta = \arctan\frac{1}{\sqrt{2}} \approx 35° \tag{7}$$

and

$$r_s^2 = \sqrt{6}/|f(t)|. \tag{8}$$

The energy of the saddle is

$$V_s = -6^{3/4} 2\sqrt{|f(t)|}. \tag{9}$$

During a field cycle the saddle moves in from infinity along the line $\theta_s = \theta$, back out to infinity, and then in and out again along the line $\theta_s = \pi - \theta$.

For the dynamics in full phase space the stability properties of the configuration are important. Since the electrons move fast compared to the frequency of the field we can employ for this analysis an adiabatic approximation and work with a constant field. Then we can scale out the field amplitude completely and put $f(t)=1$. The triangular electron configuration then becomes stationary and the dynamics near this saddle is governed by the eigenvalues of the linearization. Within the C_{3v} symmetry subspace the triangular electron configuration has one unstable direction corresponding to a crossing of the saddle. In these scaled units the Lyapunov exponent for motion along this reaction coordinate [28,29] is $\lambda_r = 1.1054$. The other eigenmode of the saddle in the subspace is stable.

Harmonic approximation in the full eight-dimensional configuration space results in three additional pairs of degenerate eigenvalues. Of these pairs two are stable and one is unstable. The unstable eigenspace points toward asymmetric configurations, has a Lyapunov exponent $\nu_a = 1.4496$, and is spanned by the vectors

$$\begin{aligned} \rho_1 &= R_s + w_a, \quad z_1 = Z_s + 2.0642 w_a, \\ \rho_2 &= R_s + w_a, \quad z_2 = Z_s + 2.0642 w_a, \\ \rho_3 &= R_s - 2.0000 w_a, \quad z_3 = Z_s - 4.1284 w_a, \end{aligned} \tag{10}$$

and

$$\begin{aligned} \rho_1 &= R_s - u_a, \quad z_1 = Z_s - 2.0642 u_a, \\ \rho_2 &= R_s + u_a, \quad z_2 = Z_s + 2.0642 u_a, \\ \rho_3 &= R_s, \quad z_3 = Z_s. \end{aligned} \tag{11}$$

The first mode describes a motion where for positive w_a two electrons move away from and one toward the nucleus or vice versa for negative w_a. The other mode leaves one electron on the saddle and brings one closer and one further out.

One may compare the period of the laser field applied in the experiments [11] with the time scales for crossing of the saddle in the C_{3v} subspace and for departure from the subspace. For peak field intensity 1.5×10^{15} W/cm^2 and for a wavelength of 795 nm, the field period [in the scaled variables (4)] is $2\pi/\omega = 33.6$ while $1/\lambda_r = 0.9$ and $1/\nu_a = 0.69$. This indicates that crossing the saddle and departure from the nonsequential triple ionization manifold take place rather quickly, justifying the adiabatic analysis *a posteriori*.

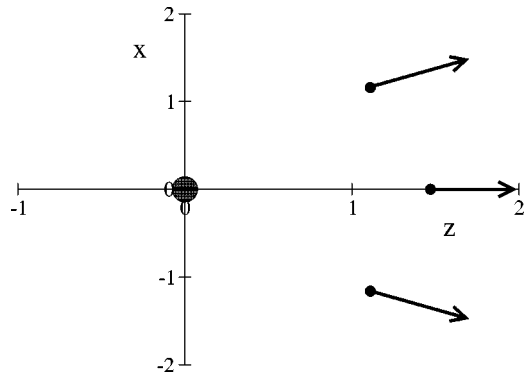

FIG. 3. Saddle in the C_{2v} symmetry subspace. The three electrons are placed at the stationary points of the potential (13) [for $Ff(t)=1$]. The arrows indicate the unstable mode of the saddle corresponding to the simultaneous escape of all electrons. The circle at the origin of the coordinate system marks the position of the nucleus.

B. C_{2v} subspace

In addition to the triangular configuration there is one with all electrons in a plane. For fixed external field the potential (2) possesses a stationary point with one electron on the polarization axis and the other two placed on either side symmetrically with respect to the field axis (Fig. 3). Without loss of generality we may assume that the electrons are confined to the x-z plane and then the C_{2v} subspace is spanned by

$$\begin{aligned} y_1 = y_2 = y_3 = 0, \\ p_{y_1} = p_{y_2} = p_{y_3} = 0, \\ x_1 = 0, \quad p_{x_1} = 0, \\ x_2 = -x_3 = x, \quad p_{x_2} = -p_{x_3} = p_x/2, \\ z_2 = z_3 = z, \quad p_{z_2} = p_{z_3} = p_z/2. \end{aligned} \tag{12}$$

The phase space for motion in this subspace is six dimensional, with variables (x,z,z_1,p_x,p_z,p_{z1}). The Hamiltonian becomes

$$H = \frac{p_x^2 + p_z^2}{4} + \frac{p_{z_1}^2}{2} - \frac{6}{\sqrt{x^2+z^2}} - \frac{3}{z_1} + \frac{1}{2|x|} + \frac{2}{\sqrt{x^2+(z-z_1)^2}} - (2z+z_1) f(t). \tag{13}$$

In contrast to the C_{3v} subspace the saddle cannot be given analytically and has to be found numerically. For $f(t)=1$, the saddle is located at $|x_s| = 1.1607$, $z_s = 1.1143$, and $z_{1,s} = 1.4665$, and has the potential energy $V_s = -7.3902$. The configuration is elongated along a line perpendicular to the field axis, with the axial position of the central electron further out than that of the outer two. Nevertheless, the distance

of the central electron to the nucleus is smaller than that of the outer electrons. It thus experiences a stronger attractive force and the balance of force requires that the other two electrons contribute a component pointing away from the nucleus, i.e., that $|z_s|<|z_{1,s}|$, as indeed observed.

Harmonic approximation in the C_{2v} subspace around the saddle reveals one stable and two unstable modes. One of the unstable directions, with Lyapunov exponent $\lambda_{2r}=1.0980$, corresponds to simultaneous escape of three electrons: in the eigenspace

$$\begin{aligned} z_1 &= z_{1,s} + w_{2r}, \\ x &= x_s + 0.6183 w_{2r}, \\ z &= z_s + 1.1417 w_{2r} \end{aligned} \tag{14}$$

all three components increase for positive w_{2r}. This eigenspace thus corresponds to the reaction coordinate in the triangular configuration. The other eigenmode

$$\begin{aligned} z_1 &= z_{1,s} + u_{2a}, \\ x &= x_s - 0.2313 u_{2a}, \\ z &= z_s - 0.3127 u_{2a} \end{aligned} \tag{15}$$

with Lyapunov exponent $\nu_{2a}=1.7937$ is related to double or single ionization, according to the sign of u_{2a}.

Harmonic approximation in the full space gives in addition to the modes within the subspace three stable modes, two unstable ones reflecting divergence from the C_{2v} subspace and one neutral mode connected with an overall rotation around the field axis. The neutral mode is connected with conservation of angular momentum and was eliminated in the C_{3v} case by transformation to polar coordinates; it shows up in the C_{2v} analysis where Cartesian coordinates are more convenient since one electron would come to lie on the singularity of the polar coordinate system. The first unstable mode with Lyapunov exponent $\nu_{2b}=0.9024$ corresponds to deviations along the y axis,

$$\begin{aligned} y_1 &= u_{2b}, \\ y_2 &= -0.5752 u_{2b}, \\ y_3 &= -0.5752 u_{2b}. \end{aligned} \tag{16}$$

The other unstable mode, with the Lyapunov exponent $\nu_{2c}=1.3712$, is related to symmetry breaking within the x-z plane,

$$\begin{aligned} x_1 &= 0.0746 u_{2c}, \quad z_1 = z_{1,s}, \\ x_2 &= x_s + 0.6598 u_{2c}, \quad z_2 = z_s + u_{2c}, \\ x_3 &= -x_s + 0.6598 u_{2c}, \quad z_3 = z_s - u_{2c}. \end{aligned} \tag{17}$$

The Lyapunov exponents are of similar magnitude as in the C_{3v} case and the adiabatic approximation remains justified.

C. Comparison between the subspaces

Analysis of the stationary points in phase space shows that there are two pathways to nonsequential triple ionization. The triangular configuration has a potential barrier [for scaled field $Ff(t)=1$] of -7.6673, slightly lower than the one -7.3902 for the saddle in the C_{2v} subspace. Therefore, for increasing energy in the compound complex, triple ionization via the triangular path becomes possible first. The triangular state is also less unstable than the C_{2v} configuration: it has a largest Lyapunov exponent for symmetry breaking perturbations of $\nu_a=1.4496$, as compared to $\nu_{2a}=1.7937$. For motion along the reaction coordinates the Lyapunov exponent of the triangular configuration is $\lambda_r=1.1054$ and thus slightly larger than $\lambda_{2r}=1.0980$ for the C_{2v} configuration. The relative phase space weight of trajectories near the symmetry subspaces is determined by a competition between motion along the reaction coordinate and amplification of deviations from symmetry [26,27]. Generally, the faster the motion along the reaction coordinate and the slower the symmetry breaking the larger the phase space that is dominated by the saddle.

There are no quantitative estimates for the phase space region influenced by the saddle, except close to a threshold, where a suitable extension of Wannier's arguments can be employed [23–25]. For triple ionization and in the presence of several symmetry breaking modes, the generalization [26,27] gives a threshold behavior $\sigma(\Delta E)\propto(\Delta E)^{\alpha}$ with exponent

$$\alpha = \left(\sum \nu_i \right) / \lambda_j, \tag{18}$$

where λ_j is the Lyapunov exponent of the reaction coordinate and the ν_i are those of the symmetry breaking modes. Specifically, for our example here we find for the triangular configuration

$$\alpha_3 = 2.6228 \tag{19}$$

and for the C_{2v} configuration

$$\alpha_2 = 3.7043. \tag{20}$$

This already suggests that the triangular configuration will be the dominant configuration. In addition to the threshold behavior the two saddles also differ considerably in the final momentum distributions of ionizing electrons, and this will be analyzed in the next section.

III. ION MOMENTA DISTRIBUTIONS

In the present section we show numerical simulations of the nonsequential ionization. We restrict our calculations to the symmetry subspaces and compare the resulting final ion momentum distributions. Even though the symmetry subspaces are of zero phase space weight and are furthermore unstable, nonsequential triple ionization trajectories in full phase space have to pass sufficiently close to the saddles and these subspaces so that they will show distributions very close to the ones obtained in the subspaces [21,22]. We can,

therefore, also compare our data with experimental distributions. In order to allow comparison with experiments we now omit the elimination of the maximal field amplitude F by the rescaling (4).

In the experiments of Moshammer *et al.* [11] on triple ionization of Ne, ultrashort (30 fs) laser pulses at 795 nm wavelength and with peak intensities of 1.5 PW/cm^2 were used. This corresponds to a frequency of $\omega=0.057$ a.u. (atomic units), a pulse duration, measured as full width at half maximum, of 11 periods $2\pi/\omega$, and a maximal field strength of $F=0.207$ a.u. Among the measured data we focus on the distributions of ion momenta parallel to the polarization axis. In the limit of negligibly small momentum transfer by the absorbed photons, the ion momentum $\vec{p}_{ion}$ reflects the sum of the momenta of the emitted electrons, $\vec{p}_{ion}=-\Sigma_i\vec{p}_i$ [7,11].

The three-electron Hamiltonian (1) corresponds to lithium. In order to relate the calculations to other atoms with more electrons, interactions with core electrons have to be neglected and the point of reference in energy has to be shifted to the threshold for triple ionization. Specifically, for the modeling of the experiments [11] on triple ionization in Ne we thus assume that in a rescattering process the energy transfer is less than the threshold for triple ionization (about 4.6 a.u.). The precise value of the energy transferred in the rescattering event and thus of the energy E of the initial compound state cannot be determined within our model and constitutes a free parameter. Similarly, the time t_0 during the pulse when the rescattering complex forms is a second free parameter. But both parameters can be determined rather reliably by comparison with experiments [22]. We now turn to the simulations within the two symmetry subspaces.

A. Simulations in the C_{3v} subspace

In a first series of simulations we focus on the triangular configuration. We fix the initial energy E and analyze the dependence of the results on the initial time t_0. To this end we chose a microcanonical distribution of initial conditions in the C_{3v} symmetry subspace for energy $E=-0.5$ a.u. and random phases ϕ for different initial time t_0. The final distributions of ion momenta parallel to the polarization axis are shown in Fig. 4. As in our previous analysis of the nonsequential double ionization process [21,22] the distributions have a double hump structure and the width of the distributions increases when the initial time t_0 approaches the peak amplitude of the field. The width of the distributions can be estimated from the maximal energy a free electron can acquire in the field, i.e., twice the ponderomotive energy. For three electrons ejected in the same direction, the corresponding maximal ion momentum depends on the amplitude of the field at the point in time when they are ionized, i.e.,

$$p_{max}=\frac{3Ff_p(t)}{\omega}, \tag{21}$$

where $f_p(t)=\sin^2(\pi t/T_d)$ is the pulse envelope. If this time is taken to equal the starting time t_0 of the simulations we find values of p_{max} that correspond very well to the widths of the

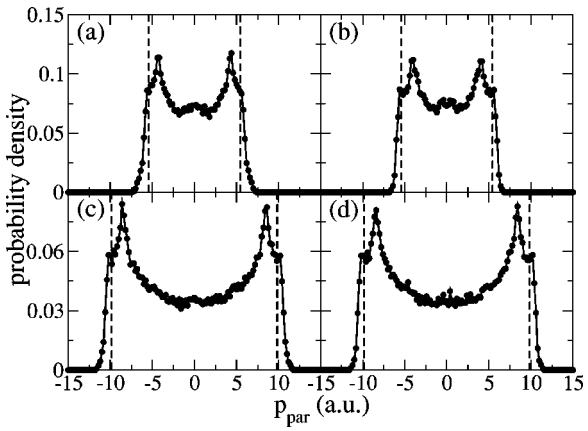

FIG. 4. Final distributions of parallel ion momenta calculated in the C_{3v} symmetry subspace for the initial energy $E=-0.5$ a.u., peak field amplitude $F=0.207$ a.u., and pulse duration $T_d=20\times2\pi/\omega$, where $\omega=0.057$ a.u. The initial times under the pulse envelope are $t_0=0.25T_d$ (a), $t_0=0.75T_d$ (b), $t_0=0.4T_d$ (c), and $t_0=0.6T_d$ (d). Dashed lines indicate the estimates $\pm3Ff_p(t_0)/\omega$. Note that the distributions are essentially the same whether one chooses t_0 before or after the peak field value, provided $f_p(t_0)$ is the same. The distributions are based on about 8×10^4 trajectories.

distributions in Fig. 4. Figure 4 indicates also that the distributions are basically the same independently of whether t_0 is chosen before or after the maximum of the pulse, provided $f_p(t_0)$ is the same. This implies that the dominant ionization takes place during the first field cycle after formation of the complex. Fitting the width of the calculated distribution to the experimental results allows one to estimate the moment in the pulse when the majority of the triply ionized ions are created.

The dependence of the ion momentum distributions on the initial energy E for fixed initial time t_0 is presented in Fig. 5. The width of the distributions does not change significantly with E but their shape does. For initial energy close to the

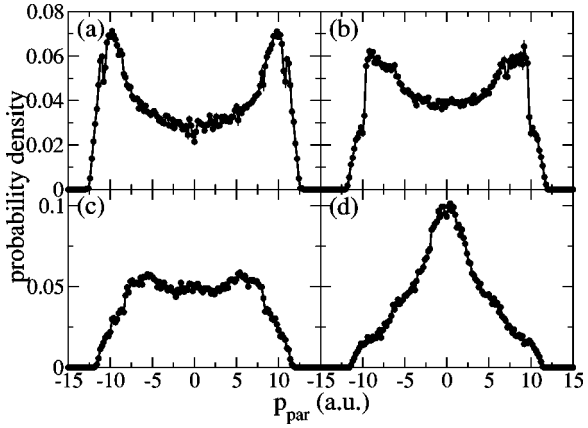

FIG. 5. Ion momentum distributions in the C_{3v} subspace for fixed initial time $t_0=0.5T_d$ and different initial energies $E=-0.05$ a.u. (a), $E=-1.5$ a.u. (b), $E=-2$ a.u. (c), and $E=-3$ a.u. (d). The parameters are the same as in Fig. 4. The minimal energy of the saddle, obtained for the maximal field amplitude, is -3.49 a.u.

minimal saddle energy, which for $F=0.207$ a.u. is -3.49 a.u., the distributions show a single maximum only, while for higher energies two humps form. The electrons that cross the saddle when the energy is near the saddle energy are slow and the combined interaction of the external and Coulomb fields shapes the distribution [22]. The situation is different for the high energy case: then shortly after the electrons cross the saddle the interaction with the electric field is stronger than the attraction to the nucleus and the distribution is mostly shaped by the laser field [22]. As the initial energy of the complex is determined in a rescattering event and is higher for stronger external fields, the distribution of ion momenta should show a transition from a distribution with a single maximum near the threshold for triple ionization to one with a double maximum higher up. For even higher fields the constraints from the triangular configuration are relaxed and less symmetric modes of triple ionization become possible.

B. Numerical simulation in the C_{2v} subspace

We now turn to the ion momentum distributions in the C_{2v} subspace. Much of the analysis proceeds as in the previous subsection, except for the difference in Hamiltonians [here it is Eq. (13)] and the choice of initial conditions. The microcanonical ensemble of the initial conditions is not straightforward to realize because (even for fixed time) for nonzero external field the system is open. In the previous section, the difficulties could be overcome by constraining initial conditions to lie on the energy shell and in the hypersurface $Z=0$ (for details see [22]). Here such a restriction is not sufficient, and phase space remains open. The troublesome configurations are those where electron distances to the nucleus are strongly asymmetric, one being close and two far away, or vice versa. Since we assume that the initial state is formed during a rescattering and should be confined to a region close to the core, such configurations cannot be formed. We therefore choose initial conditions microcanonically and require in addition that distances of the electrons to the nucleus are not larger than the minimal distance of the saddle at maximal field to the nucleus.

As in the previous section, the width of the momentum distributions determines the initial time t_0 when triple ionization takes place. The dependence on initial energy E is also similar, with a collapse of all structures into a single peak near zero momentum as the initial energy decreases toward the energy of the saddle (Fig. 6).

In Fig. 6 we show final parallel ion momentum distributions corresponding to nonsequential triple ionization in the C_{2v} subspace for three different initial energies E. The structure of the distributions is significantly different from that in the previous section. In Fig. 6(a) and 6(b), in addition to two local maxima on the edges of the distributions, a strong contribution appears at zero momentum value that is split into two maxima. The origin of these structures can be related to qualitatively different electron paths. Initially, after crossing the saddle all three electrons escape toward the same side of the nucleus. However, the final momenta along the polarization axis may point in either the same or opposite directions,

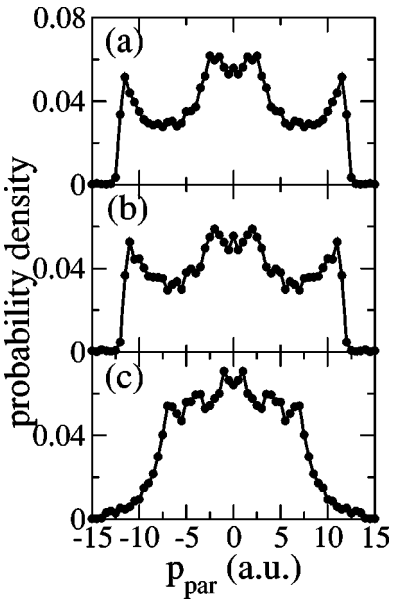

FIG. 6. Final distributions of parallel ion momenta calculated for nonsequential triple ionization in the C_{2v} symmetry subspace for the peak field amplitude $F=0.207$ a.u., pulse duration $T_d=20\times 2\pi/\omega$ (where $\omega=0.057$ a.u.), and initial time in the pulse duration $t_0=0.5T_d$. The initial energy is $E=-0.05$ a.u. (a), $E=-0.5$ a.u. (b), $E=-2$ a.u. (c) and the minimal energy of the saddle is -3.36 a.u. The distributions are obtained from a few thousand trajectories.

depending on the initial conditions and the phase of the field, as shown in Fig. 7. If the final momenta point in the same direction, they can be much larger than if they point in opposite directions. Therefore, the edge maxima are the effect of the electrons escaping toward the same direction while the central structure corresponds to escape in opposite directions.

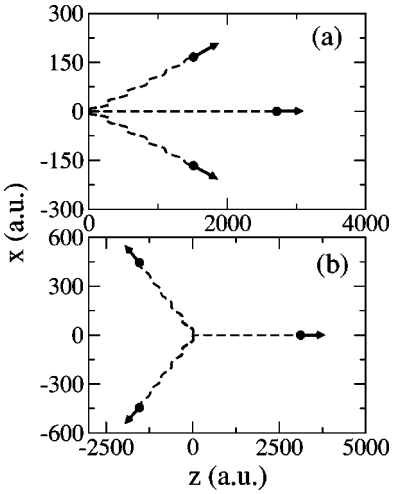

FIG. 7. Examples of trajectories corresponding to simultaneous three-electron escape by crossing the saddle in the C_{2v} symmetry subspace. The electrons, when crossing the saddle, move initially toward the positive z direction (the saddle in both cases is located at $z>0$). However, depending on the phase of the field, their final momenta can point in either the same (a) or opposite (b) directions.

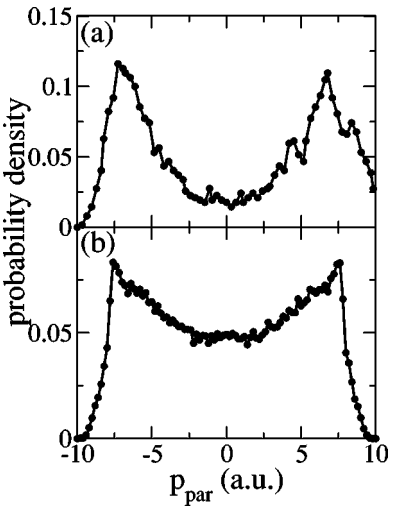

FIG. 8. Comparison between experimental (a) and numerical (b) ion momenta. Ion momentum distributions are from the experiment of [11] on triple ionization of Ne atoms in the focus of 795 nm, 30 fs (i.e., about $11\times 2\pi/\omega$) laser pulses at peak intensity of 1.5 PW/cm^2 (i.e., peak field strength $F=0.207$ a.u.). The numerical distributions are for the C_{3v} symmetry subspace with initial energy $E=-1$ a.u. and $t_0=0.33T_d$ where $T_d/2=11\times 2\pi/\omega$ [see Eq. (3)].

C. Comparison with experiment

Given the qualitatively very different distributions of final ion momenta in the two subspaces we can use a comparison with experimental data [11] to draw conclusions about the dominant ionization mode. In Fig. 8 we show the experimental parallel ion momentum distribution together with the one calculated from the C_{3v} symmetry subspace. In the calculation we have chosen the initial time $t_0=0.33T_d$ that gives a width of the resulting distribution in agreement with the experiment. The initial energy has been taken as $E=-1$ a.u. but it can be taken in a wide range of values above -1.5 a.u. without significant changes in momentum distributions (Fig. 5). The main features of the experimental distribution are well reproduced in our calculations. However, the minimum in the distribution is less pronounced than that observed in the experiment. Overall, we take this good agreement as strong indication that triple ionization occurs in the neighborhood of the symmetric process discussed here.

The distributions for perpendicular ion momenta, which have been measured in the experiment [11], cannot be calculated within the symmetry subspace since this component vanishes exactly by symmetry. In full phase space ionizing electrons pass close to the saddle but not exactly symmetrically and consequently the transverse ion momenta do not vanish.

IV. CONCLUSION

We have considered the pathways along which a highly excited three-electron complex can decay toward triple ionization. In nonsequential multiple ionization of atoms in strong laser fields such a complex forms when the rescattered electron collides with the core. The subsequent nonsequential decay then has to follow the pathways discussed here. We found two possible pathways, one proceeding via a symmetric triangular configuration, and one via a planar elongated configuration. A stability analysis shows that the ionization close to the C_{3v} symmetry subspace occurs at lower field intensities and has a larger cross section (close to threshold). Trajectory simulations within this subspace give final ion momentum distributions in very good agreement with the recent experimental data [11]. The C_{2v} configuration has a higher threshold and smaller cross section and gives a momentum distribution different from the experimentally observed one, so that we conclude that the triangular configuration is indeed the dominant one.

We have not discussed pathways to sequential triple ionization, and one can expect that there are several, including sequential ionization of one electron after the other, a double ionization followed by a single ionization, or the other way around, or various combinations of partial ionizations and rescatterings. As in the case of double ionization [21,22], one can also have sequential ionization from failed attempts to triple ionize along one of the symmetric saddles. The experimental results of [11] suggest that, at least in the intensity range considered here, correlated nonsequential electron escape dominates. This is further supported by our previous analysis of double ionization [22], where we found that the double hump structure observed in the experimental ion momentum distributions [7–11] does not appear in the sequential process. That is, the electron momenta are not correlated and the resulting distributions show a strong single maximum instead of the double hump structure.

Finally, let us mention that part of our analysis can be easily extended to nonsequential multiple ionization where the number of escaping electrons N is greater than 3 [21]. The triangular configuration extends to placement of electrons on a ring with C_{Nv} symmetry in the plane perpendicular to the field axis. Calculation of the positions and the energy of the saddle shows that the energy is nonmonotonic and begins to increase with increasing N for more than nine electrons. For more than 13 electrons the saddle does not exist any more. Therefore, for many electrons the configurations with highest symmetry will disappear and others will dominate the ionization process. For triple ionization we have identified one, the planar configuration, and for more than three electrons we expect a rapidly increasing number of stationary configurations. The identification of a dominant pathway will then require an appropriate stability analysis and an application of the generalized Wannier threshold law [26,27].

ACKNOWLEDGMENTS

We would like to thank H. Giessen, W. Becker, R. Kopold, and H. Rottke for discussions. Financial support by the Alexander von Humboldt Foundation and KBN under Project No. 5 P03B 088 21 is gratefully acknowledged.

[1] *Super-Intense Laser-Atom Physics*, Proceedings of the NATO Advanced Research Workshop, Han-sur-Lesse, Belgium, 1993, edited by B. Piraux, A. L'Huillier, and K. Rzążewski (Plenum, New York, 1993).
[2] *Super-Intense Laser-Atom Physics*, Proceedings of the NATO Advanced Research Workshop, in Han-sur-Lesse, Belgium, 2000, edited by B. Piraux and K. Rzążewski (Kluwer Academic Publishers, Dordrecht, 2001).
[3] A. L'Huillier, L. A. Lompre, G. Mainfray, and C. Manus, Phys. Rev. A **27**, 2503 (1983).
[4] K. C. Kulander, K. J. Schafer, and J. L. Krause, in *Super-Intense Laser-Atom Physics* (Ref. [1]), p. 95.
[5] P. B. Corkum, Phys. Rev. Lett. **71**, 1994 (1993).
[6] K. C. Kulander, J. Cooper, and K. J. Schafer, Phys. Rev. A **51**, 561 (1995).
[7] Th. Weber, M. Weckenbrock, A. Staudte, L. Spielberger, O. Jagutzki, V. Mergel, F. Afaneh, G. Urbasch, M. Vollmer, H. Giessen, and R. Dörner, Phys. Rev. Lett. **84**, 443 (2000).
[8] Th. Weber, M. Weckenbrock, A. Staudte, L. Spielberger, O. Jagutzki, V. Mergel, F. Afaneh, G. Urbasch, M. Vollmer, H. Giessen, and R. Dörner, J. Phys. B **33**, L128 (2000).
[9] Th. Weber, H. Giessen, M. Weckenbrock, G. Urbasch, A. Staudte, L. Spielberger, O. Jagutzki, V. Mergel, M. Vollmer, and R. Dörner, Nature (London) **405**, 658 (2000).
[10] Th. Weber, M. Weckenbrock, A. Staudte, M. Hattass, L. Spielberger, O. Jagutzki, V. Mergel, H. Böcking, G. Urbasch, H. Giessen, H. Bräuning, C. Cocke, M. Prior, and R. Dörner, Opt. Express **8**, 368 (2001).
[11] R. Moshammer, B. Feuerstein, W. Schmitt, A. Dorn, C. D. Schöter, J. Ullrich, H. Rottke, C. Trump, M. Wittmann, G. Korn, K. Hoffmann, and W. Sandner, Phys. Rev. Lett. **84**, 447 (2000).
[12] A. Becker and F. H. M. Faisal, J. Phys. B **29**, L197 (1996).
[13] A. Becker and F. H. M. Faisal, J. Phys. B **32**, L335 (1999).
[14] B. Sheehy, R. Lafon, M. Widmer, B. Walker, L. F. DiMauro, P. A. Agostini, and K. C. Kulander, Phys. Rev. A **58**, 3942 (1998).
[15] A. Becker and F. H. M. Faisal, Phys. Rev. A **59**, R1742 (1999).
[16] A. Becker and F. H. M. Faisal, Phys. Rev. Lett. **84**, 3546 (2000).
[17] R. Kopold, W. Becker, H. Rottke, and W. Sandner, Phys. Rev. Lett. **85**, 3781 (2000).
[18] B. Feuerstein, R. Moshammer, and J. Ullrich, J. Phys. B **33**, L823 (2000).
[19] M. Lein, E. K. U. Gross, and V. Engel, Phys. Rev. Lett. **85**, 4707 (2000).
[20] J. Chen, J. Liu, L. B. Fu, and W. M. Zheng, Phys. Rev. A **63**, 011 404(R) (2001).
[21] B. Eckhardt and K. Sacha, Phys. Scri. **T90**, 185 (2001).
[22] K. Sacha and B. Eckhardt, Phys. Rev. A **63**, 043 414 (2001).
[23] G. H. Wannier, Phys. Rev. **90**, 817 (1953).
[24] A. R. P. Rau, Phys. Rep. **110**, 369 (1984).
[25] J. M. Rost, Phys. Rep. **297**, 271 (1998).
[26] B. Eckhardt and K. Sacha (unpublished).
[27] J. M. Rost, Physica E **9**, 467 (2001).
[28] E. P. Wigner, Z. Phys. Chem. Abt. B **19**, 203 (1932); Trans. Faraday Soc. **34**, 29 (1938).
[29] E. Pollak, in *Theory of Chemical Reactions*, edited by M. Baer (CRC Press, Boca Raton, FL, 1985), Vol III, p. 123.